# Transition-Metal Nanocluster Kinetic and Mechanistic Studies Emphasizing Nanocluster Agglomeration: Demonstration of a Kinetic Method That Allows Monitoring of All Three Phases of Nanocluster Formation and Aging

Brooks J. Hornstein and Richard G. Finke*

*Department of Chemistry, Colorado State University, Fort Collins, Colorado 80523*

*Received July 4, 2003. Revised Manuscript Received October 26, 2003*

A kinetic method following the development, and then the loss, of catalytic activity is used to monitor the nucleation, growth, and then pyridine or acetonitrile-induced *agglomeration* (also called aggregation, coagulation, or flocculation) of modern, catalytically active Ir(0) nanoclusters stabilized by $P_2W_{15}Nb_3O_{62}^{9-}$ polyoxoanions and $Bu_4N^+$ cations in acetone. The agglomeration kinetics of the Ir(0) nanoclusters are shown to fit an often assumed, but rarely experimentally determined, bimolecular aggregation step, B + B → C, rate constant $k_3$, where B is the active catalyst and C is the deactivated catalyst. When this agglomeration step is added to the previously determined slow, continuous nucleation A → B, rate constant $k_1$, and then autocatalytic surface growth, A + B → 2B, rate constant $k_2$, steps (A is the (1,5-COD)Ir(I)$^+$ in the precatalyst), the full steps of nucleation, growth, and then agglomeration are followed and treated kinetically for the first time for a modern, prototype transition-metal nanocluster. A pictorial scheme depicting these three pseudo-elementary steps is also presented. The treatment of agglomeration kinetics is significant since it should permit additional, important advances, specifically, the ready recognition of agglomeration, the measurement of the agglomeration rate constant $k_3$, and, especially, the quantitative study of agglomeration, $k_3$, as a function of all the variables that stabilize or destabilize transition-metal nanoclusters (e.g., added ligands, solvents of different dielectric constant or coordinating ability, different anions or cations, added polymers or dendrimers, and so on). Additional insights generated by these studies are also discussed. Last, presented as targets of future research are the unexplained observations: (a) that the Ir(0) nanoclusters are not agglomerated by the added salt of noncoordinating anions such $Bu_4N^+BF_4^-$, contrary to the salt-induced agglomeration observed for classical colloids where primarily DLVO (Derjaguin−Landau−Verway−Overbeek)-type Coulombic repulsion vs van der Waals attractive forces are operative; and (b) that the Ir(0) and other, selected modern transition-metal nanoclusters in organic solvents may be taken to dryness and then fully redissolved, that is, do not appear to possess a ccc (critical coagulation concentration) as do water-soluble, DLVO-stabilized classical colloids.

## Introduction

**Prior Studies of Colloidal Agglomeration.** Studies of agglomeration[1−6] (also called aggregation, coagulation, or flocculation) are central to understanding the stability of colloidal or modern nanocluster materials.[7] Indeed, as Turkevich has noted,[2] aggregation studies of colloids provided early, historically important evidence for the very existence of the colloidal state. Since the classic studies by Smoluchowski[1] and then Turkevich,[2,3] two limiting regimes of agglomeration kinetic behavior have been known, diffusion-limited[1−8] and chemical reaction-process-limited.[2,4−6] Fractal geometry products are common if not the rule.[5] Smoluchowski's theory treats diffusion-controlled agglomeration adequately, but deviations for slow, reaction-process-limited agglomeration have been observed by several workers as summarized by Turkevich.[2a]

* To whom correspondence should be addressed. E-mail: rfinke@lamar.colostate.edu.

(1) von Smoluchowski, M. *Phys. Z.* **1916**, *17*, 557 and 585.

(2) (a) Enüstün, B. V.; Turkevich, J. *J. Am. Chem. Soc.* **1963**, *85*, 3317. See also refs 4−9, 11, 12, and 14 therein reporting deviations from Smoluchowski theory in the case of slow aggregation (rates faster than predicted or coagulation that stops completely at a certain stage). (b) Turkevich, J. *Gold Bull.* **1985**, *18*, 125. If they have not already done so, readers interested in nanocluster science will want to read this somewhat buried, but classic, Part II mini-review as well as the earlier Part I, Turkevich, J. *Gold Bull.* **1985**, *18*, 86.

(3) In his pioneering studies, Turkevich used transmission electron microscopy (TEM) to obtain a modest amount of data following the coagulation of large (400 nm), dilute Au/citrate$^{3-}$ colloids. Agglomeration was induced by salt addition and added gelatin was employed to arrest the agglomeration so that samples for TEM could be obtained. (a) Turkevich, J. *Am. Sci.* **1959**, *47*, 97. (b) Baker, C.; Turkevich, J. U.S. Atomic Energy Commission Report, NYO-3436. (c) A concise overview of these studies is given on 126−128 of ref 2b (Part II) cited herein.

10.1021/cm034585i CCC: $27.50 
Published on Web 12/13/2003

However, quantitative kinetic studies of agglomeration of even classical colloids are not routine, in part due to the paucity of methods to follow conveniently and quantitatively the agglomeration of colloids in real time.[6,9] The use of light-scattering methods to monitor agglomeration can be problematic if not controversial[4h] due to the non-monodispersity of particles present, the possibility of multiple scattering,[4a,6a] or even the subtle effects of the shear forces of simple dilution on the resultant particle aggregation state.[4a] TEM is another possible, but inconvenient, method for studying nanocluster distributions as a function of time,[3] one that provides relatively few data points of uncertain accuracy even in the best cases. Indeed, establishment of the empirical rate law of agglomeration in terms of the colloid or nanocluster concentration has almost never been done; instead, an irreversible process *and* second-order kinetics are typically *assumed*.[1,2,6] Under these two assumptions, the average *radius* or *mass* formation exhibits power-law kinetics for a diffusion-limited process and exponential kinetics for reaction-rate controlled agglomeration.[5a,8] Experimental demonstration of the rate law for agglomeration in terms of the mechanistically more useful *concentration* of nanoclusters—that is, the rate law needed for a chemical understanding of the nucleation, growth, and agglomeration mechanism—remains as an important experimental objective,[6f] one addressed herein.

**Prior Studies of Nanocluster Agglomeration.** Quantitative kinetic studies of agglomeration of *modern nanoclusters*[7] are essentially unknown[10] due to the lack of well-defined, prototype systems until the past decade[7,11] as well as the aforementioned problems in following agglomeration in real time. In no case that we can find is a detailed, approaching molecular-level mechanism for agglomeration of a transition-metal nanocluster or colloid available that includes anything approaching elementary (or pseudo-elementary, vide infa) steps and supporting kinetic evidence. This is as expected at this time, however, due to the inherent complexity of aggregation processes.[12] More quantitative, more readily interpretable kinetic and mechanistic studies are one area where modern transition-metal nanoclusters hold significant potential to make fundamental contributions to our understanding of the forma-

(4) Other agglomeration lead references: (a) Gregory, J. In *Nanoparticles in Solids and Solutions*; Fendler, J. H., Dékány, I., Eds.; Kluwer Academic Publishers: Dordrecht, 1996; pp 203−255 ("Particle Agglomeration: Modeling and Measurement). (b) Meakin, P. *Adv. Colloid Interface Sci.* **1988**, *28*, 249−331 and references therein. ("Fractal Aggregates"). (c) Ross, S.; Morrison, I. D. *Colloidal Systems and Interfaces*; John Wiley: New York, 1988; Chapter IIID, p 255 ("Kinetics of Coagulation"). (d) Granqvist, C. G.; Buhrman, R. A. *J. Catal.* **1976**, 42, 477; this paper details a log-normal size distribution of supported particles due to aggregative growth. (e) Tojo, C.; Blanco, M. C.; Rivadulla, F.; López-Quintela, M. A. *Langmuir* **1997**, *13*, 1970. Monte Carlo kinetic simulations assuming diffusive nucleation and growth. (f) A review titled "Kinetic Models of Colloid Aggregation" with 57 references covering aggregation "models" (basically Smoluchowski's model[1]) and "simulations" (Monte Carlo methods, molecular dynamics, Brownian dynamics, and others): Gardner, K. H. *Surf. Sci. Ser.* **1999**, *85*, 509−550. (g) Ag agglomeration in poly(methyl methacrylate): Yanagihara, N. *Chem. Lett.* **1998**, *4*, 305−306. (h) For a case where the true cause for the changes in light scattering seen upon diluting Au colloids was debated as being due to the shear forces of simple dilution, vs the possibility of multiple scattering, see: Wilcoxon, J. P.; Marin, J. E.; Schaefer, D. W. *Phys. Rev. Lett.* **1987**, *58*, 1051. Weitz, D. A.; Lin, M. Y.; Lindsay, H. M.; Huang, J. S. *Phys. Rev. Lett.* **1987**, *58*, 1052.

(5) Additional[2b,6a] studies of fractal aggregates: (a) Lin, M. Y.; Lindsay, H. M.; Weitz, D. A.; Ball, R. C.; Klein, R.; Meakin, P. *Nature* **1989**, *339*, 360. Note that by "universality in colloid aggregation" these authors use "universal" in the fractal sense; that is "independent of the specific details of how the particular particles are formed". (b) For an introduction to fractal growth see: Sander, L. M. *Sci. Am.* **1987**, *256* (Jan), 94.

(6) Additional[2,3] lead references to kinetic studies of agglomeration of transition-metal colloids are the following. Note that Au, Ag, and Cu are relatively easy systems to monitor since their plasmon resonance appears in the visible region of the electromagnetic spectrum. (a) A classic paper on pyridine-induced agglomeration of Au colloids: Weitz, D. A.; Huang, J. S.; Lin, M. Y.; Sung, J. *Phys. Rev. Lett.* **1985**, *54*, 1416. See also the discussion therein about the issues in using light scattering to follow colloidal agglomeration, issues of polydispersity and whether the Born approximation for weak scattering is satisfied. (b) Pyridine-induced Au colloid agglomeration: Blatchford, C. G.; Campbell, J. R.; Creighton, J. A. *Surf. Sci.* **1982**, *120*, 435. (c) Pyridine-induced Au colloid agglomeration: Weitz, D. A.; Huang, J. S. In *Kinetic of Aggregation and Gelation*, Proceedings of the International Topical Conference on Kinetics of Aggregation and Gelation, April 2−4, 1984, Athens, Georgia; Family, F., Landau, D. P., Eds.; Elsevier: Amsterdam, 1984; pp 19−27. (d) Ag nanoparticle agglomeration: Van Hyning, D. L.; Klemperer, W. G.; Zukoski, C. F. *Langmuir* **2001**, *17*, 3128. (e) A paper which provides important kinetic evidence for a bimolecular Pd(0) catalyst decomposition as a sidelight of the main, oxidation catalysis focus of the paper: Steinhoff, B. A.; Fix, S. R.; Stahl, S. S. *J. Am. Chem. Soc.* **2002**, *124*, 766. (f) A valuable paper which treats $TiO_2$ colloid agglomeration in an unstirred solution as reversible and by a second-order agglomeration rate law is: Vorkapic, D.; Matsoukas, T. *J. Colloid Interface Sci.* **1999**, *214*, 283. Regarding the lack of nanoclusters concentration vs time data in the literature, a relevant quote in this paper is: "...the available data are usually limited to size measurements." (g) Although not transition-metal colloids, a paper on the aggregation kinetics of dendrimer-stabilized CdS nanoclusters has appeared: Hanus, L. H.; Sooklal, K.; Murphy, C. J.; Ploehn, H. J. *Langmuir* **2000**, *16*, 2621.

(7) (a) For definitions of modern nanoclusters, and their differences from classical colloids,[7b] see: Finke, R. G. In *Metal Nanoparticles: Synthesis, Characterization and Applications*; Feldheim, D. L., Foss, C. A., Jr., Eds.; Marcel Dekker: New York, 2002; Chapter 2, pp 17−54. (b) Classical colloids, in comparison to modern nanoclusters, typically (i) are larger in size (>10 nm, (ii) have broader size distributions (≫15%), (iii) have a poorly defined molecular composition, (iv) are not isolable and redissolvable, (v) are not reproducibly prepared, (vi) have irreproducible catalytic activities (often ≥500%[7c]), (vii) contain surface-bound, rate-inhibiting species such as $X^-$, $O^{2-}$, $OH^-$, and $H_2O$, and (viii) historically have been $H_2O$, but not organic solvent, soluble. (c) Köhler, J. U.; Bradley, J. S. *Catal. Lett.* **1997**, *45*, 203−208.

(8) Melrose, J. R. *J. Chem. Phys.* **1990**, *92*, 4595. Melrose's paper is of interest to the present work since he treated the surface-area dependence of a redox reaction under surface-limiting ("slow") and diffusion-limiting ("fast") agglomeration conditions. A power law in time for the reaction rates with exponents $\alpha/d_f - 1$ (i.e., $t^{\alpha/d_f-1}$) and $1/d_f - 1$ (i.e., $t^{1/d_f-1}$)for the two cases was derived, where $d_f$ = the fractal dimension and $t$ = time.

(9) A critical review of particle-size measurement methods: Miller, B. F.; Lines, R. W. *Crit. Rev. Anal. Chem.* **1988**, *20*, 75−116.

(10) (a) Consistent with this statement, we scoured the literature for a published data set on the concentration of nanoclusters vs time that we could fit, as a control experiment, to the nucleation, growth, and agglomeration kinetic scheme herein. *We could not find a suitable nanocluster concentration vs time data set in the literature that we could use in such a control experiment.* (b) An initial study of nanocluster agglomeration under $H_2$ mass-transfer limitations has appeared: Aiken, J. D., III; Finke, R. G. *J. Am. Chem. Soc.* **1998**, *120*, 9545.

(11) Additional lead reviews of modern transition-metal nanoclusters: (a) Aiken, J. D., III; Finke, R. G. *J. Mol. Catal. A: Chem.* **1999**, *145*, 1. (b) Schmid, G.; Baumle, M.; Geerkens, M.; Heim, I.; Osemann, C.; Sawitowski, T. *Chem. Soc. Rev.* **1999**, *28*, 179. (c) Schmid, G.; Chi, L. F. *Adv. Mater.* **1998**, *10*, 515. (d) Fendler, J. H., Ed.; *Nanoparticles and Nanostructured Films*; Wiley-VCH: Weinheim, 1998. (e) Aiken J. D., III; Lin, Y.; Finke, R. G. *J. Mol. Catal. A: Chem.* **1996**, *114*, 29. (f) Fürstner, A., Ed.; *Active Metals: Preparation, Characterization, and Applications*; VCH: Weinheim, 1996. (g) Bradley, J. S. In *Clusters and Colloids. From Theory to Applications*; Schmid, G., Ed.; VCH: New York, 1994; pp 459−544. (h) Schmid, G. *Chem. Rev.* **1992**, *92*, 1709. (i) A superb series of papers, complete with a record of the insightful comments by the experts attending the conference, is available. *Faraday Discuss.* **1991**, *92*, 1−300. (j) Schmid, G. In *Aspects of Homogeneous Catalysis*; Ugo, R., Ed.; Kluwer: Dordrecht, 1990; Chapter 1. (k) Andres, R. P.; Averback, R. S.; Brown, W. L.; Brus, L. E.; Goddard, W. A., III; Kaldor, A.; Louie S. G.; Moscovits, M.; Peercy, P. S.; Riley, S. J.; Siegel, R. W.; Spaepen, F.; Wang, Y. *J. Mater. Res.* **1989**, *4*, 704. (l) Henglein, A. *Chem. Rev.* **1989**, *89*, 1861. (k) Thomas, J. M. *Pure Appl. Chem.* **1988**, *60*, 1517. (m) Jena, P.; Rao B. K.; Khanna, S. N. *Physics and Chemistry of Small Clusters*; Plenum: New York, 1987.

tion and agglomeration of nanoclusters and colloids.[7] This follows from the better defined compositions and reproducible preparations and properties of nanoclusters vs traditional colloids.[7,13]

**Factors Affecting the Stability of Colloidal and Nanocluster Materials.** Understanding what accelerates or slows agglomeration is central to understanding the *stability* of colloidal and nanocluster materials. The stability of colloids and nanoclusters is known to be due in significant part to surface-adsorbed anions;[14,15] the resultant anionic charge provides particle stability due to electrostatic repulsion between colloidal particles of the same, multiple charge. That repulsion is opposed by van der Waals attractions between the particles, the competition between these two effects being the basis for the classic Derjaguin−Landau−Verway−Overbeek (DLVO) theory of colloid stability from the 1940s.[14] Added good ligands, notably pyridine,[6a−c] lead to colloid agglomeration by displacing the coordinated anions, thereby lowering the electrostatic repulsion barrier and permitting faster agglomeration. Added high concentrations of electrolyte[2,14] also cause agglomeration by compaction the double- (really multi-)[14], Debye layer surrounding colloidal particles, thereby leading to closer particle−particle contact and, ultimately, agglomeration. The ability of high salt concentrations or pyridine to induce agglomeration is taken as good evidence for the DLVO mode of colloid stabilization as are measurements which indicate the colloid's overall charge (i.e., electrophoretic or $\zeta$-potential measurements[14]). Such studies to establish the particle's overall surface charge are well-established for water-soluble, classical colloids but are rare in modern transition-metal nanoclusters.[11] A case where the overall anionic charge to the otherwise neutral Ir(0) nanocluster core[16] has been established is that of $P_2W_{15}Nb_3O_{62}^{9-}$ polyoxoanion-stabilized nanoclusters. The pyridine-induced agglomeration of these same, modern nanoclusters[7] will be studied herein.

**Important Issues in the Agglomeration of Modern Transition-Metal Nanoclusters.** Important but previously unanswered questions for the agglomeration of modern transition-metal nanoclusters include, then, the following: (i) Will first- or second- (or possibly higher) order aggregation processes dominate?; (ii) Is any agglomeration detectable when the current top (poly)anionic stabilizer,[15] the $P_2W_{15}Nb_3O_{62}^{9-}$ polyoxoanion, is used along with a top stabilizing solvent (e.g., the high dielectric constant solvent propylene carbonate ($\epsilon = 69$)), but in the absence of any added agglomerating agent such as pyridine?[17−19]; (iii) Is, however, ready agglomeration seen when only the weakly coordinating,[20] and thus weakly stabilizing, $BF_4^-$ anion is present (again without added pyridine; if so, this will then provide additional evidence for an anion-based, DLVO-type of stabilization of modern nanoclusters)?; (iv) Can agglomeration be induced by pyridine or high salt concentrations (e.g., added $Bu_4N^+BF_4^-$) even for highly stabilized nanoclusters, for example, our $P_2W_{15}Nb_3O_{62}^{9-}$ and propylene carbonate-stabilized Ir(0) nanoclusters, thereby offering a classic piece[7,16] of evidence for DLVO-theory type of Coulombic repulsion stabilization, due to surface-adsorbed anions, in modern transition-metal nanoclusters? Perhaps most significantly, (v) Can agglomeration be added to the prior demonstration of the mechanism of formation for transition-metal nanoclusters from metal−salt precursors, A, consisting of[21] slow, continuous *nucleation*, A → B (rate constant $k_1$), then autocatalytic surface *growth*, A + B → 2B (rate constant $k_2$), where B is the catalytically active metal(0) on the growing nanocluster's surface? That is, can bimolecular agglomeration, B + B → C (agglomerated product; rate constant $k_3$), be added to the above to steps to describe *the full kinetics of modern nanocluster nucleation, growth, and agglomeration for the first time*? Experimental measurement and then quantitative accounting for the kinetics of this expected three-component mechanism of formation and then agglomeration

(12) A quote from Meakin's review[4b] is telling about the inherent complexity of aggregation phenomena: "Aggregation in most real systems involves a wide range of physical and chemical processes including long- and short-range interactions (van der Waals forces, screened electrostatic interactions, steric effects, hydrodynamic interactions, etc.), adsorption and desorption of ions and neutral species, chemical bond formation, sintering, bridging, etc. In addition, a variety of processes can occur during and after aggregation. These include structural reorganization, reversible aggregation, and chemical processes. In addition, many aggregation processes involve particles with a broad range of sizes, shapes, and compositions. The aggregating particles may also have a complex surface geometry and large heterogeneities in their surface chemistry. It is clear that incorporation of all these (and many other) effects (such as the change in the solvent structure near to the particle surface) into a single model would be a formidable undertaking."

(13) Studies of agglomeration are directly related to the issue of the factors that stabilize nanoclusters. A couple of interesting quotes in this regard are as follows: (a) "Although electrostatic stability has been one of the oldest and most important issues in colloidal science, *the number of studies that are sufficiently systematic to be useful is limited*" (italics have been added). Hirtzel, C. S.; Rajagopalan, R. *Colloidal Phenomena*: *Advanced Topics*; Noyes Publications: Park Ridge, NJ, 1985; pp 27−39/73−87. (b) "Little is known as to how conventional ligands and other ingredients stabilize metal colloids during a given "homogeneous process". Such knowledge would set the scene for the directed application of "colloidal ligands". Both the theory of colloids (formation, structure, stabilization) and their catalytic performance will clearly form a center of gravity of future research." *Applied Homogeneous Catalysis with Organometallic Compounds: A Comprehensive Handbook in Two Volumes*; Cornilis, B., Herrmann, W. A., Eds.; Volume 1: Applications, 1996; Chapter 4.1.2 ("Colloidal Organometallic Catalysis").

(14) For a general discussion on the stability of colloids or nanoclusters, see, for example: (a) Evans, D. F.; Wennerström, H. *The Colloidal Domain*, 2nd ed.; Wiley-VCH: New York, 1999. (b) Hirtzel, C. S.; Rajagopalan, R. *Colloidal Phenomena*: *Advanced Topics*; Noyes Publications: Park Ridge, NJ, 1985; pp 27−39/73−87. (c) Hunter, R. J. *Foundations of Colloid Science*; Oxford University Press: New York, 1987; Vol. 1, pp 316−492.

(15) (a) Özkar, S.; Finke, R. G. *J. Am. Chem. Soc.* **2002**, *124*, 5796. (b) Özkar, S.; Finke, R. G. *Langmuir* **2002**, *18*, 7653.

(16) (a) Lin, Y.; Finke, R. G. *J. Am. Chem. Soc.* **1994**, *116*, 8335. (b) Lin, Y.; Finke, R. G. *Inorg. Chem.* **1994**, *33*, 4891.

(17) Reetz and co-workers were the first to report that propylene carbonate might be a preferred solvent for stabilizing nanoclusters: Reetz, M. T.; Lohmer, G. *J. Chem. Soc., Chem. Commun.* **1996**, 1921−1922.

(18) Scaled-up, isolated Ir(0) nanoclusters stabilized by the $P_2W_{15}Nb_3O_{62}^{9-}$ polyoxoanion, propylene carbonate, and $Bu_4N^+$ counterions: Hornstein, B. J.; Finke, R. G. *Chem. Mater.* **2003**, *15*, 899.

(19) Additional studies are underway of the factors affecting the stability of modern transition-metal nanoclusters, including solvents, cations, polymers, dendrimers, siloxanes, and other claimed stabilizers: Starkey, L.; Finke, R. G. Unpublished results and experiments in progress.

(20) (a) Rosenthal, M. R. The myth of the noncoordinating anion. *J. Chem. Educ.* **1973**, *50*, 331. (b) Lawrance, G. A. *Chem. Rev.* **1986**, *86*, 17−33. (c) Strauss, S. H. *Chem. Rev.* **1993**, *93*, 927−942.

(21) (a) Watzky, M. A.; Finke, R. G. *J. Am. Chem. Soc.* **1997**, *119*, 10382. This paper, together with our 2001 paper,[21d] provides a comprehensive listing of the prior literature of the mechanisms of particle nucleation and growth. (b) Watzky, M. A.; Finke, R. G. *Chem. Mater.* **1997**, *9*, 3083. (c) Aiken, J. D., III; Finke, R. G. *J. Am. Chem. Soc.* **1998**, *120*, 9545 and references therein to diffusive agglomeration of nanoparticles. (d) Widegren, J. A.; Aiken, J. D., III; Özkar, S.; Finke, R. G. *Chem. Mater.* **2001**, *13*, 312, and references therein.

of modern transition-metal nanoclusters has not been previously accomplished despite its anticipated significance. For example, adding agglomeration to the mechanism of formation, then aging, of modern transition-metal nanoclusters is expected to be quite valuable: (a) for screening stabilizers (do they inhibit agglomeration?); (b) for quantitative measurements of $k_3$, and hence of stability and agglomeration, as a function of different synthesis and reaction conditions; and overall (c) for extracting the true $k_1$, $k_2$, and now also $k_3$ values. A knowledge of the three rate constants governing transition-metal nanocluster nucleation, growth, and agglomeration ($k_1$, $k_2$, and $k_3$) as a function of the multiple variables affecting these rate constants (i.e., as a function of the different anions, solvents, cations, polymeric stabilizers, and temperatures employed for nanocluster formation and stabilization) is of far-reaching, fundamental significance.

Herein, we report the needed studies to address questions (i)−(v) above for our prototype Ir(0) nanoclusters.[15,16,19,21,25,27,30,33] The system by which we form the nanoclusters[15,16,18] in eq 1 allows us to study agglomeration in the desired extreme cases of the best documented anionic stabilizer, $P_2W_{15}Nb_3O_{62}^{9-}$,[15] but then also the minimal anionic stabilization afforded by the weakly basic, weakly coordinating $BF_4^-$ anion. We demonstrate that pyridine induces agglomeration when even the $P_2W_{15}Nb_3O_{62}^{9-}$ polyoxoanion is the stabilizer, thereby providing additional evidence[15,16] for a DLVO-type of adsorbed-anion-based stabilization of a modern transition-metal nanocluster. Overall, the complete kinetic curve involving nucleation, growth, and agglomeration is quantitatively accounted for, opening the door to the needed further studies and advances noted in (a)−(c) above. Such studies are only possible since they build off our earlier studies of the A → B nucleation and then A + B → 2B autocatalytic surface-growth kinetics and mechanism of transition-metal nanocluster formation from metal salts under $H_2$.[21]

## Results and Discussion

**The Nanocluster Formation Reaction.** Generally speaking, the Ir(0) nanoclusters are formed as before,[21] from the well-established reaction shown in eq 1, where $Y^-$ is a general anion, 1,5-COD is 1,5-cyclooctadiene, and PS is the Brønsted base Proton Sponge, a preferred $H^+$ scavenger in nanocluster formation reactions:[15b]

$$[Bu_4N]_qY + [(1,5\text{-COD})Ir(CH_3CN)_2]BF_4 + PS + 2.5\,H_2 \xrightarrow[40\ \text{psig}\ H_2]{\text{acetone, 22 °C}}$$

$$\bigcirc + 1/n\ \{[Bu_4N]_{nq}[Ir(0)_n \bullet nY]\} + PS\text{-}H^+ + 2CH_3CN + BF_4^- \qquad (1)$$

In the case of the $Y^- = P_2W_{15}Nb_3O_{62}^{9-}$ stabilized nanoclusters, we begin as before[15,16] with the precatalyst complex, $[Bu_4N]_5Na_3[(1,5\text{-COD})Ir{\cdot}P_2W_{15}Nb_3O_{62}]$, **1**, formed via eq 1 from $[Bu_4N]_9P_2W_{15}Nb_3O_{62}]$ plus $[(1,5\text{-COD})Ir(CH_3CN)_2]BF_4$ and then isolated.[15] While not absolutely necessary, the available[16] preformed complex **1** is the preferred precursor since it gives the most exact control over the $Ir(I)/P_2W_{15}Nb_3O_{62}^{9-}$ ratio, which in turns leads to the most reproducible kinetic behavior.[15] Hence, we have employed **1** in the present studies.

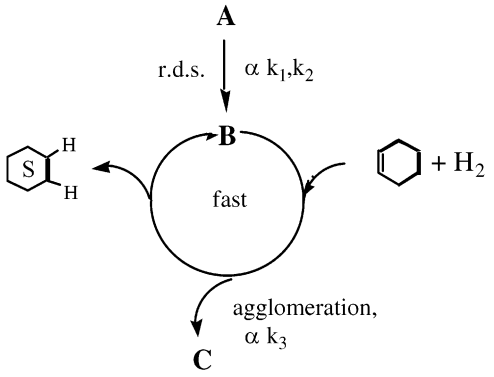


**Figure 1.** Illustration of how transition-metal nanocluster formation is monitored via the fast, follow-up catalytic reaction of cyclohexene hydrogenation by the nanocluster catalyst, **B**. As before,[21] **A** is the $[(1,5\text{-COD})Ir(I)]^+$-containing precatalyst, **B** is the active $Ir(0)_n$ in the nanocluster hydrogenation catalyst, and **C** is the agglomerated, inactive, former **B**. The rate constants $k_1$, $k_2$, and $k_3$ are defined via eqs 3a−3c in the text, vide infra.

**Pseudo-Elementary Step Kinetic Method[21] and Use of a Pressure Transducer To Follow the $H_2$ Loss.** To understand the agglomeration studies which follow, it is necessary to understand the indirect, but rapid, quantitative, and real-time kinetic method by which we follow our nanocluster's formation and, herein, their agglomeration. The method is one that we developed in a series of papers;[21a−d] it employs the fact that the catalytic activity of the nanoclusters is proportional to the concentration of the active Ir(0) metal, B, that is, $-d[H_2]/dt = -d[\text{cyclohexene}]/dt \propto [B]$,[1] as shown in Figure 1 where A in Figure 1 is, in general, the $[(1,5\text{-COD})Ir(I)]^+$ complex, for example, A = **1** in the case where $P_2W_{15}Nb_3O_{62}^{9-}$ is the anionic stabilizer:

Given in eqs 2−4 which follow are the precise overall stoichiometry in the case beginning with A = **1**, eq 2, the individual kinetic steps (eqs 3a−3d), and then their summation to the pseudo-elementary step[21] shown in eq 4. Generally speaking, a pseudo-elementary step is just the summation of a few slow steps, in the present case three slow steps (eqs 3a−3c), plus one or more fast steps (eq 3d), to yield the desired pseudo-elementary step, eq 4, in the present case.[21] The beauty and power of a pseudo-elementary step is that it can be used in kinetics analogous to the way a truly elementary step is used. Specifically, one can write the following relations from eq 4 that are essential to the analysis of the kinetic data: $(1/(1 - y))(d[B]/dt) = (1/1400)(-d[\text{cyclohexene}]/dt)$ (when the reaction is run, as it is herein, with 1400 equiv of cyclohexene compared to the initial 1 equiv of A). That is, one can monitor the loss of cyclohexene (or, by eq 4, more conveniently and equivalently monitor the loss of $H_2$) *yet measure the kinetics of the desired steps of nucleation ($k_{1obs}$), growth ($k_{2obs}$), and agglomeration ($k_{3obs}$) as the Ir precatalyst A is converted into catalytically active Ir(0) nanoclusters, B, and then agglomerated into C (= inactive B).* Of note here is that this kinetic method allows the use of a sensitive (±0.01 psig) pressure transducer to follow the loss of hydrogen (which, again, can be equated to the loss of cyclohexene given their 1:1 stoichiometry, eq 4), thereby allowing the rapid collection of *a wealth of high-precision kinetic data* for use in probing the mechanism of transition-metal nanocluster formation, the factors

affecting the stability of those nanoclusters, and as studied herein, nanocluster agglomeration. The $H_2$ pressure data have a precision of approximately ±0.03% (i.e., ±0.01 psig/40 psig total monitored = ±0.03%).

$$300[(1,5\text{-COD})Ir{\cdot}P_2W_{15}Nb_3O_{62}]^{8-} + 750H_2 + 300PS \rightarrow Ir(0)_{\sim 300}{\cdot}(P_2W_{15}Nb_3O_{62}{}^{9-})_{\sim 66} + 300\text{cyclooctane} + 300PS{-}H^+ + \sim 234[P_2W_{15}Nb_3O_{62}]^{9-} \quad (2)$$

$$x[A \xrightarrow[H_2]{k_1} B] \quad (3a)$$

$$(1-x)[A + B \xrightarrow[H_2]{k_2} 2B] \quad (3b)$$

$$^1/_2[B + B \xrightarrow{k_3} 2(1-y)B + 2yC] \quad (3c)$$

$$\sim 1400[B + \text{cyclohex}\textit{ene} + H_2 \xrightarrow{\text{fast}} B + \text{cyclohex}\textit{ane}] \quad (3d)$$

---

$$\underline{\text{SUM:}}\ A + \sim 1400\ \text{cyclohex}\textit{ene} + \sim 1400H_2 \xrightarrow{k_{obs,SUM}} (1-y)B + yC + \sim 1400\ \text{cyclohex}\textit{ane} \quad (4)$$

The essence of this minimal kinetic scheme is the now well-precedented, slow, continuous nucleation step 3a, plus autocatalytic surface-growth step 3b, plus the *fast* cyclohexene reporter reaction, step 3d.[21] The differences from before[21] are that we have added the agglomeration step,[10] 3c, so that the net reaction stoichiometry is changed to eq 4. The reader probably has realized that eq 3c can be simplified to $yB \rightarrow yC$; this simplification appears in the overall stoichiometry in eq 4, but has been left as given in eq 3d since we will find that the observed kinetics are fit by a second-order, not a first-order, rate law, vide infra—that is, (3d) is a (pseudo)-elementary step. The steps (3a)−(3d) and (4), as well as their kinetic treatment, are strictly analogous to those we published earlier, except that agglomeration has been added, eq 3c, so that the equation numbers are, therefore, necessarily different from before[21] due to the addition of (3c). There is necessarily also a slightly different rate constant nomenclature used herein in comparison to our earlier nanocluster nucleation and growth kinetics papers;[21] the present nomenclature is that we recommend and henceforth will use.

Note that we have previously validated this indirect but powerful new kinetic method for following nanocluster formation (i.e., when agglomeration was not present) by showing that the $k_1$ and $k_2$ obtained by the above method is *identical within experimental* error to the $k_1$ and $k_2$ *obtained by monitoring the cyclooctane evolution* afforded by eq 2 by GC (and once the 1400 correction factor required by the mathematics in that case is made[21]). The cyclooctane evolution kinetic method is closer to being direct, but provides many fewer data points that are also of much lower precision (±15% vs the ±0.03% of the pressure transducer); it also takes a much greater time commitment to collect that inferior precision GC data, making it clear that the preferred method for performing the kinetic studies is to follow the $H_2$ loss and use eq 4 to treat the resultant data.[21] The well-understood assumptions behind the use of the pseudo-elementary step kinetic method in eq 4 are listed in a footnote for the interested reader.[22] The detailed mathematics behind the use of eq 4 and the pseudo-elementary step method plus MacKinetics numerical integration for the present case (vide infra) are provided in Appendix A. The key kinetic equation that results and which is used to measure $k_{1obs}$, $k_{2obs}$, and $k_{3obs'}$ (and, from these, $k_1$, $k_2$, and $k_3$, vide infra) is provided in eq 5 (which is also eq A.6(c) in the derivation in Appendix A). Equation 5 which follows will likely not be obvious by inspection; hence, a derivation is provided in Appendix A of the Supporting Information.

$$-\text{d[cyclohexene]}/\text{d}t = k_{1obs}[A]_t + k_{2obs}[A]_t[B]_t + k_{3obs}[B]_t^2 \quad (5)$$

where $[A]_t$ = [cyclohexene]$_t$ and $[B]_t = \{[\text{cyclohexene}]_0 - [\text{cyclohexene}]_t\}$and where $k_1 = (1 - y)k_{1obs}$, $k_2 = 1400k_{2obs}$, and $k_3 = [(1400)/(1 - y)]\ k_{3obs}$ Also, in a substitution that simplifies the MacKinetics curve fitting procedure, the equation B + B → C′ (rate constant $k_{3obs'}$; note the prime after "3obs") is used rather than the physically and mechanistically more correct, pseudoelementary step eq 3c shown earlier, B + B → 2(1 − *y*)B + 2*y*C. However, the desired $k_{3obs}$ (and then from it, $k_3$) is readily obtained from the relationship $k_{3obs} = (2/y)k_{3obs}$, which is derived in Appendix A, eq A.15.

**Control of High Stabilization Conditions: $P_2W_{15}Nb_3O_{62}{}^{9-}$-Stabilized Nanoclusters in Acetone.** As previously reported, exposure of a solution containing 20 mg of **1**, 2.5 mL of acetone, and 0.5 mL of cyclohexene to 40 psig $H_2$ results in the formation of $Ir(0)_{\sim 300}$ nanoclusters that are 2.0 ± 0.3 nm in size and are completely soluble in acetone, acetonitrile, and propylene carbonate. The formation of these nanoclusters is accompanied by a sigmoidally shaped loss of cyclohexene that can be fit to an analytic equation derived from

(22) The approximations, assumptions, or proper techniques behind the use of the pseudo-elementary step kinetic method in eq 4 include (i) that the [olefin] dependence is zero order (this has been shown to be true initially under our Standard Conditions,[21a] but it is certainly not true toward the end of the reaction where the olefin is eventually completely consumed) and (ii) that the $H_2$ pressure is, ideally, constant since a first-order dependence on $pH_2$ has been demonstrated previously[21a] (this is certainly not true throughout the whole reaction since one is following the loss of $pH_2$; however, as noted and treated before,[21a] if one sets up an experiment in which, as an example, 20 psig had to be followed to obtain the needed data (i.e., a case of facile agglomeration with lots of added pyridine, for example), then the error introduced would be a tolerable, ca. ±33% error due to treating the initial 40 psig $pH_2$ as an average $pH_2 = 30 \pm 10$ psig). In addition, the kinetic treatment (iii) assumes that nanoclusters of different size or surface structure have the same, size-independent rate of hydrogenation reaction (i.e., that each of $k_1$, $k_2$, and $k_3$ is independent of nanocluster size). This assumption is again not 100% true, but again is a very workable assumption as discussed in our original paper,[21a] especially since the *structure-insensitive reaction* of olefin hydrogenation was deliberately picked from the beginning so that this condition is met in-so-far as possible (see the discussion of this point elsewhere[21a]). No new approximations are introduced by adding the agglomeration step in eq 3d and rate constant $k_3$. We do note, however, that (iv) $k_3$ measures the loss of catalytically active sites by all pathways that may be present; that is, $k_3$ includes any surface deactivation processes that may be occurring (although this looks to be a slower process[18]). In the end, and although the methods herein provide a previously unavailable way to follow nanocluster agglomeration, the resultant $k_3$ in these initial, deliberately unoptimized experiments should be considered as most reliable when *relative* $k_3$ values are being compared.

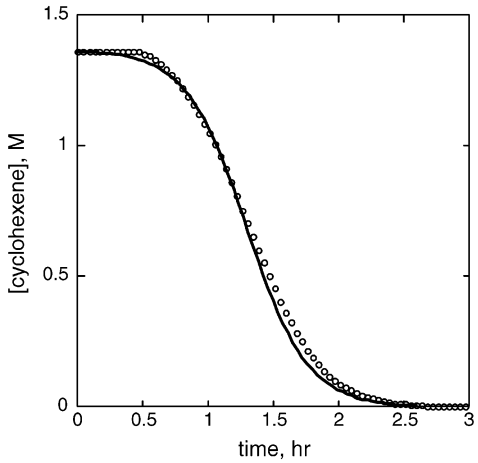


**Figure 2.** Plot of [cyclohexene] vs time for a Standard Conditions synthesis of $Ir(0)_{\sim 300}$ nanoclusters (open circles). Reaction conditions: 20 mg of $[Bu_4N]_5Na_3[(1,5\text{-COD})Ir{\cdot}P_2W_{15}Nb_3O_{62}$ (**1**), 2.5 mL of acetone, 0.5 mL of cyclohexene, 40 psig $H_2$, 22 °C. The solid line is a fit obtained from Origin using the analytic expression derived from eqs 3a and 3b for the autocatalytic mechanism. The fit via numerical integration of eqs 3a and 3b, accomplished with MacKinetics (see the Experimental Section), is indistinguishable from that carried out using Origin and the integrated, analytic expressions corresponding to eqs 3a and 3b. Table 1 lists the resultant $k_{1,obs}$ and $k_{2,obs}$ rate constants.

**Table 1. Data Showing Agreement in the Fit Values Obtained by Origin vs MacKinetics**

| fitting program | equations used in kinetic model[a] | $k_{1obs}$ ($h^{-1}$)[b] | $k_{2obs}$ ($M^{-1}$ $h^{-1}$)[b] | $k_{3obs'}$ ($M^{-1}$ $h^{-1}$) |
|---|---|---|---|---|
| Origin 3.5 | 3a, 3b | 0.022 | 2.85 | |
| MacKinetics | 3a, 3b | 0.021 | 2.89 | |
| MacKinetics | 3a, 3b, 3c | 0.021 | 2.90 | $(\sim 1 \times 10^{-5})$[c] |

[a] Equations refer to those in the main text. [b] Error bars from the reproducibility of the curve fits were typically less than or equal to ±10−20%, while the reproducibility of repeat experiments was typically less than or equal to ±20%; see the Experimental Section as well as footnote 22 for further details. [c] This $k_{3obs}$ value is small (and thus less-well determined or determinable), within experimental error of zero.

(only) eqs 3a and 3b (i.e., no eq 3c, $k_{3obs}$ term is necessary for an excellent fit). These data and curve fit are shown in Figure 2 and the values of $k_{1obs}$ and $k_{2obs}$ are reported in Table 1.

To make sure that the values for $k_{1obs}$ and $k_{2obs}$ obtained from the analytic equation (i.e., Origin) are the same as those obtained with the numerical integration algorithm of MacKinetics, the same data set in Figure 2 was fit with MacKinetics. The results are given in Table 1 and show that both software packages give the same values within experimental error.

Although both fitting programs give satisfactory fits to the experimental data in the absence of agglomeration, the fit values and the fit quality obtained with MacKinetics are quite sensitive to the initialization parameters. If random initial parameters are entered into MacKinetics, the fitting procedure requires many iterations and often gives nonsensical (e.g., negative) values for the rate constants. In light of this observation, initial guesses for $k_{1obs}$ and $k_{2obs}$ were made based on fits to the analytic equations as carried out with Origin. For experiments that showed agglomeration, this procedure was also used, but only the first half of the data were fit with Origin, thereby minimizing any contribution from agglomeration, $k_{3obs}$, to the resultant $k_{1obs}$ and $k_{2obs}$ initial guesses.

An additional curve-fitting control experiment was carried out to test if the addition of eq 3c to the kinetic model changes the values of $k_{1obs}$ and $k_{2obs}$ in a case where "no" agglomeration, $k_{3obs'}$ = ca. 0, is believed to be the case. Specifically, agglomeration via eq 3c was incorporated into the kinetic model and the data in for the polyoxoanion stabilizer, Figure 2, were re-fit with MacKinetics. *A negligible value for $k_{3obs'}$ is observed* ($k_{3obs'} \sim 1 \times 10^{-5}$ $M^{-1}$ $s^{-1}$). This control experiment confirms the previously believed lack of agglomeration with the $P_2W_{15}Nb_3O_{62}^{9-}$ polyoxoanion "Gold Standard" anionic stabilizer[15] in acetone at 22 °C. This control also confirms that, at least in the absence of any kinetically or TEM-detectable agglomeration, the values of $k_{1obs}$ and $k_{2obs}$ are not affected (i.e., are free from artifacts) caused by fitting data to a kinetic model that includes agglomeration, eq 3c and rate constant $k_{3obs'}$ even when detectable agglomeration is absent.

**Pyridine-Induced Agglomeration.** The Ir(0) nanoclusters stabilized by $P_2W_{15}Nb_3O_{62}^{9-}$ in acetone involve a high, record level of anion-based stablization.[15,17−19] Hence, it is of considerable interest to see if added pyridine or $[Bu_4N]BF_4$ induces agglomeration of such nanoclusters.

When a "Standard Conditions"[15] hydrogenation experiment was carried out in the presence of pyridine beginning with the complex, $[Bu_4N]_5Na_3[(1,5\text{-COD})Ir{\cdot}P_2W_{15}Nb_3O_{62}]$, **1**, a fine black precipitate of bulk metal is observed (i.e., as a final form of agglomerated nanoclusters, "C", eq 3c)—*demonstrating unequivocally that agglomeration has occurred since only discrete nanoclusters are formed in the absence of pyridine, vide supra*. TEM of the *soluble portion* of the reaction mixture shows nanoclusters 1.6 ± 0.4 nm in diameter (Figure S1, Supporting Information), a size within experimental error of the nanoclusters obtained without pyridine. This is further unequivocal evidence that (a) nanoclusters were formed and (b) that they then agglomerated to the observed bulk metal. (The literature suggests that the bulk metal is composed of dense fractal aggregates in such well-stirred solutions with their resultant shear forces.[5,8]) In addition, the kinetics are now *not* fit by the kinetic model involving *only* nucleation and growth (eqs 3a and 3b). Attempted fits to either all the data, or just the first half of the data, using only eqs 3a and 3b are shown in Figure 3. Comparing those results with the (much better) fit obtained from a kinetic model that includes the agglomeration step, eq 3c, Figure 4, provides strong evidence that agglomeration, eq 3c and $k_3$, is *required* for a satisfactory fit to the experimental data. The resultant values for the rate constants $k_{1obs}$, $k_{2obs}$, and $k_{3obs'}$ are listed in Table 2.

Although the fit in Figure 4 is quite good, the calculated concentration values do deviate from the experimental at *long times* when the [cyclohexene] approaches zero. This deviation is indicative of the breakdown of the assumption necessary in the pseudo-elementary step treatment of[22] $-d[\text{cyclohexene}]/dt \propto [\text{cyclohexene}]^0$. For this reason, the $k_{3obs}$ values obtained herein, which are necessarily obtained from the fuller

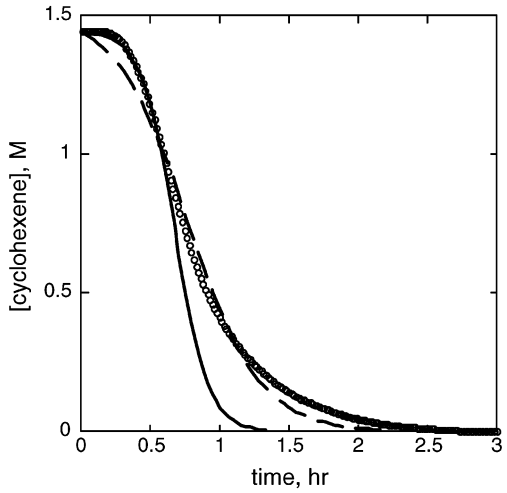


**Figure 3.** Plot of [cyclohexene] vs time for the formation of polyoxoanion-stabilized Ir(0) nanoclusters synthesized from the complex, $[Bu_4N]_5Na_3[(1,5\text{-COD})Ir{\cdot}P_2W_{15}Nb_3O_{62}]$, **1**, in the presence of 2 equiv of pyridine. Reaction conditions: 20.0 mg of **1**, 2.5 mL of acetone, 0.5 mL of cyclohexene, 2 equiv of pyridine, 40 psig $H_2$, 22 °C. The experimental data are the open circles while the dashed and solid lines are the fits to a kinetic model without aggregation (i.e., using only eqs 3a and 3b) using all the data (the dashed line) or only the first half of the data (the solid line). Rather clearly, this "no agglomeration" model provides a relatively poor fit of the data, especially relative to Figure 4 when agglomeration is included and where a much better fit is seen (vide infra).

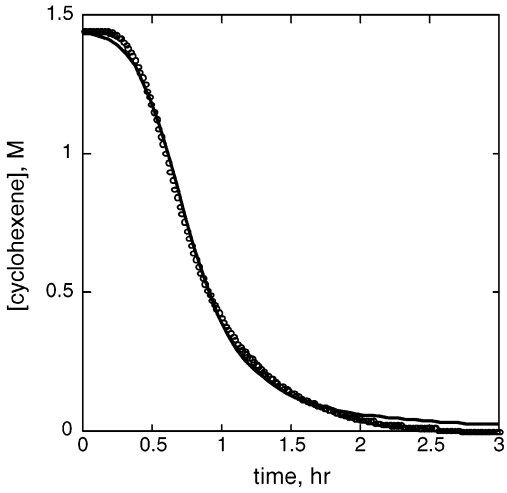


**Figure 4.** Plot of [cyclohexene] vs time for the formation of polyoxoanion-stabilized Ir(0) nanoclusters synthesized from **1** in the presence of 2 equiv of pyridine. Reaction conditions: 20.0 mg of **1**, 2.5 mL of acetone, 0.5 mL of cyclohexene, 40 psig $H_2$, 22 °C. The experimental data (open circles) are well-fit by a kinetic model that includes bimolecular agglomeration (solid line).

data set at longer times (i.e., where agglomeration can predominate), contain some systematic error in their absolute values and should be considered semiquantitative estimates of the true $k_3$ *for these particular experiments*.[22] However, this is quite acceptable at this time (a) since this is the first such kinetic demonstration of agglomeration for modern transition-metal nanoclusters, (b) since the agglomeration kinetic data that result can still be used to rank nanocluster stabilizers (since the systematic error should tend to cancel), and especially (c) since future studies can be designed to minimize the error. Smaller errors can be realized by using higher olefin concentrations or less precatalyst, **A**, by using more pyridine and thereby studying faster agglomeration for a shorter time that consumes less cyclohexene, and by also fitting less of the full sigmoidal curve in cases where agglomeration is more prevalent (i.e., with higher [pyridine], weaker stabilizers, or in less stabilizing solvents, for example). Under these latter conditions, the approximations detailed in a footnote[22] are better satisfied.

An important, more general point here that while it is important to strive for small-molecule like precision and accuracy (i.e., ±15% rate constants) for nanocluster nucleation, growth, and agglomeration reactions, the nature of such complex, multistep systems is such that one can expect larger error bars and reduced precision. This is neither unexpected nor unprecedented: one finds, for example, lower precision in the *R* value for protein vs small molecule structures or the *m*/*z* value in the mass spectrometry of larger molecules such as 10 000 MW polymers (the latter being simply a function of the width of the *m*/*z* envelope observed); see p 26−28 elsewhere[7a] for a discussion of this important point for the studies of supramolecular systems.

Figure 5 shows the concentrations of precursor A, catalyst B, and agglomerated, deactivated catalyst C as a function of time as computed via MacKinetics using the $k_{1obs}$, $k_{2obs}$, and $k_{3obs'}$ values in Table 2. The resultant three concentration profiles for A, B, and C in Figure 5 have the general shapes of a classic A → B → C consecutive reaction sequence, as expected from eqs 3a−3c and the overall stoichiometry in eq 4, with the required exception that the conversion of A to B is autocatalytic, A + B → 2B, and, hence, sigmoidal.

To further quantify the $k_3$ values, an experiment was carried out to estimate the value for *y* in eq 4 for agglomeration induced by 2 equiv of pyridine. As detailed in Appendix A, an estimate of *y* can be obtained via the catalytic activity of the completely formed nanoclusters in the presence of pyridine and the catalytic activity of the completely formed nanocluster in the absence of pyridine, $y = \{[\text{catalytic activity w/o py}] - [\text{catalytic activity w/py}]/[\text{catalytic activity w/o py}]\}$. Under the conditions described in the Experimental Section, the activity of completely formed nanoclusters without pyridine is 39.7 psig $H_2$/h and the activity of completely formed nanoclusters with pyridine is 21.8 psig $H_2$/h; this leads to $y = 0.45$. This estimated *y* value allows one to convert $k_{1obs}$, $k_{2obs}$, and $k_{3obs'}$ to the $k_1$, $k_2$, and $k_3$ values listed in Table 2.

One can readily obtain a rough idea of just how much the nanocluster's size would have to increase to account for a loss of surface area corresponding to a $y = 0.45$ value (and under the assumption that all the surface sites were active, something that significantly overestimates the few percent of active metals recently titrated atop a Rh(0) nanocluster's surface[23]). Using the formula for so-called "magic number" (i.e., full shell) nanoclusters (see the formula and references cited in Figure 5 elsewhere[11e]), plus the formula for the number of Ir atoms in a given diameter nanocluster provided in footnote 29a elsewhere,[16a] it is readily calculated that our ∼20 Å, $Ir(0)_{\sim 300}$ nanoclusters (approximated by the

(23) Hornstein, B. J.; Aiken, J. D., III; Finke, R. G. *Inorg. Chem.* **2002**, *41*, 1625.

**Table 2. Summary of Rate Constants from Kinetics that Include Agglomeration**

| experiment[a] | $k_{1obs}$[d] ($h^{-1}$) | $k_{2obs}$[d] ($M^{-1}$ $h^{-1}$) | $k_{3obs'}$[d] ($M^{-1}$ $h^{-1}$) | $k_{3obs}$ ($M^{-1}$ $h^{-1}$) | $k_1$ ($h^{-1}$) | $k_2$ ($M^{-1}$ $h^{-1}$) | $k_3$ ($M^{-1}$ $h^{-1}$) |
|---|---|---|---|---|---|---|---|
| **1**, 2 equiv of pyridine in acetone[b] | 0.023 | 4.49 | 1.5 | 6.7 | 0.041 | 6290 | 17000 |
| **1**, 7 equiv of pyridine in acetone | 0.049 | 5.04 | 11.4 | | | | |
| (1,5-COD)Ir($CH_3CN$)$_2BF_4$ in acetonitrile[c] | 0.074 | 3.13 | 2.6 | | | | |

[a] Reaction conditions: 2.5 mL of solvent, 0.05 mL of cyclohexene, 40 psig $H_2$, 22 °C. [b] For this reaction, under these conditions, $y \approx 0.45$. [c] One equivalent of Proton Sponge was added. [d] Error bars from the reproducibility of the curve fits were typically less than or equal to ±10−20% while the reproducibility of repeat experiments was typically less than or equal to ±20%; see the Experimental Section as well as footnote 22 for further details.

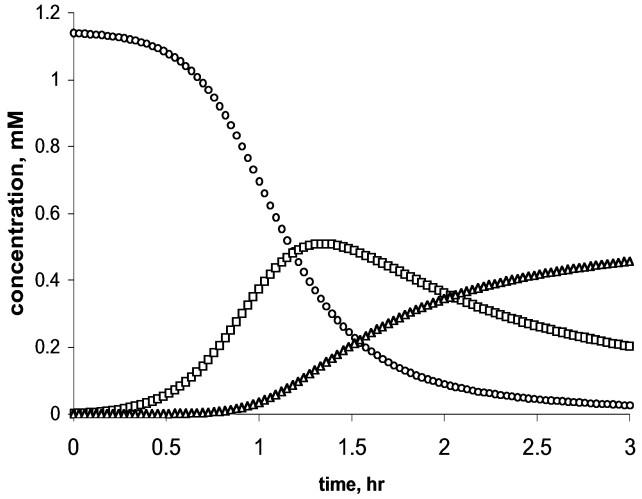


**Figure 5.** Concentration vs time plot of precursor **A** (circles), nanocluster catalysts **B** (squares), and agglomerated, deactivated catalyst **C** (triangles) for the experiment generating nanoclusters from **1** in the presence of 2 equiv of pyridine. The rate constants $k_{1obs}$, $k_{2obs}$, and $k_{3obs'}$ were used to generate this plot using MacKinetics (see the Experimental Section for further details).

magic number of 309 metal atoms), with ∼52% of their atoms on the surface, would have to agglomerate to a product "C", eq 3c, of ∼43 Å average size, Ir(0)$_{\sim 2900}$ nanoclusters (approximated by the magic number of 2869 metal atoms) which have 28% of the Ir(0) atoms on the surface. This rough calculation is useful in that it teaches that a $y = 0.45$ value for the 2 equiv of pyridine corresponds to *only a moderate level of agglomeration*.

Table 2 also includes the results of an experiment carried out in the presence of more pyridine (7, rather than 2, equiv). As in the previous py experiment, incorporation of the agglomeration step into the kinetic model is required to fit the data, Figure S3, Supporting Information. Note that this experiment shows that the rate of agglomeration is dependent on the concentration of pyridine as one would expect for an agglomeration mechanism that is reaction- rather than diffusion-controlled.[6a]

It is worth recalling at this point that electrophoretic evidence demands that the $P_2W_{15}Nb_3O_{62}^{9-}$ polyoxoanion is coordinated to the surface of the Ir(0) nanocluster.[16] Hence, an added bonus of the present pyridine-induced agglomeration studies is that they confirm[15,16] DLVO theory type of anionic stabilization of the resultant Ir(0) nanoclusters by surface-bound $P_2W_{15}Nb_3O_{62}^{9-}$ anions. This follows since pyridine induces agglomeration[6a−c,13,14] by displacing anions bound to the nanoclusters' surface (i.e., even the highly charged, strongly coordinating, and record-stabilizing $P_2W_{15}Nb_3O_{62}^{9-}$ polyanion), thereby removing anion-based, Coulombic repulsion between nanoparticles that is a central part of DLVO theory of colloidal stabilization. Modern transition-metal nanoclusters are, therefore, stabilized by DLVO-type forces as expected[14] and as we have shown,[15,16] although the anion-based stabilization of nanoclusters is little demonstrated and often ignored (e.g., as discussed in footnotes 14−16 elsewhere[15a]).

**Attempted [*n*-Bu$_4$N]BF$_4$-Induced Agglomeration.** Agglomeration of at least aqueous colloids by added salts is well-established in the colloidal literature.[14] The effect of added salts is explained as one of electrostriction of the multilayer, thereby allowing the colloidal particles to become closer together where van der Waals attractive forces then lead to more rapid agglomeration.[14] Hence, we attempted to agglomerate the Ir(0) nanoclusters with excess [*n*-Bu$_4$N]BF$_4$—note the deliberate use of the weakly coordinating anion $BF_4^-$ so as to minimize any specific anion effects (i.e., any direct displacement of the nanocluster-coordinated $P_2W_{15}Nb_3O_{62}^{9-}$ polyoxoanion by the added $BF_4^-$). Interestingly, reactions carried out in the presence of up to 0.5 M [*n*-Bu$_4$N]BF$_4$ (in acetone) *failed to show signs of agglomeration* (the kinetics were nicely fit using only eqs 3a and 3b and the reaction solutions remained clear with no visible signs of agglomeration resulting in bulk-metal precipitation). Actually, this is what we anticipated, given our earlier observation that polyoxoanion-stabilized nanoclusters,[18] as well as a number of other modern transition-metal nanoclusters,[11] lack a so-called critical coagulation concentration (ccc; see footnote 43 elsewhere[15a]) in that they can be taken to dryness and then subsequently fully redissolved in a number of organic solvents. This unusual characteristic of *modern transition-metal nanoclusters* in organic solvents distinguishes them from classical, generally less stable, *nonisolable nanocolloids* in aqueous solvents.[7] It is not obvious, however, why added $R_4N^+X^-$ salts do not lead to nanocluster agglomeration in organic solvents. Steric stabilization by the coordinated stabilizer is one possible reason for the added stability as are non-DLVO-stabilization forces.[24] Rather clearly, all the reasons behind the stability of modern transition-metal nanoclusters[14,15,17,19] in organic solvents are still not well understood and are, therefore, important targets for additional research.

**Demonstration of Agglomeration in a Weakly Coordinating Anion Case, $BF_4^-$, in the Also Less**

(24) For lead references to the growing literature on "non-DLVO forces" see: (a) Ninham. B. W. *Adv. Colloid Interface Sci.* **1999**, *83*, 1−17. Noteworthy therein is the list of 8 assumptions of DLVO theory. (b) Boström, M.; Williams, D. M. R.; Ninham, B. W. *Phys. Rev. Lett.* **2001**, *87*, 168013. (c) Grasso, D.; Subramaniam, K.; Butkus, M.; Strevett, K.; Bergendahl, J. *Re/Views Environ. Sci. Bio/Technol.* **2002**, *1*, 17−38.

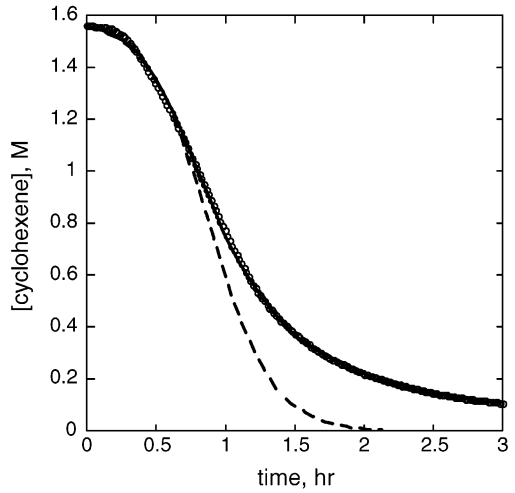


**Figure 6.** Plot of [cyclohexene] vs time for the reaction starting with (1,5-COD)Ir($CH_3CN$)$_2BF_4$ *in acetonitrile*. Reaction conditions: 1.7 mg of (1,5-COD)Ir($CH_3CN$)$_2BF_4$, 1 equiv of Proton Sponge, 2.5 mL of acetonitrile, 40 psig $H_2$, 22 °C. The open circles are the measured data, the solid line is a fit to the kinetic model that includes bimolecular agglomeration, and the dashed line is a fit to a kinetic model without agglomeration. Rather clearly, agglomeration is needed to account for, and to provide an excellent fit to, the experimental data.

**Stabilizing Solvent, Acetonitrile.** If the kinetic methods to assay agglomeration developed herein are more general, then they should be applicable to other cases, for example, the more common case of less effective stabilizers than $P_2W_{15}Nb_3O_{62}^{9-}$ and in other solvents. Hence, we tested our kinetic methods on some data generated as part of studies to assay what solvents and other conditions are best for nanocluster stabilization,[19] studies that produced the previously unpublished cyclohexene vs time curve in Figure 6 for (1,5-COD)Ir($CH_3CN$)$_2BF_4$ in acetonitrile without any other stabilizers save the $BF_4^-$ anion and its $Bu_4N^+$ countercation. The kinetics of this reaction are fit only if one includes nanocluster agglomeration, Figure 6; the dashed line in Figure 6 is an attempted fit without agglomeration. Moreover, bimolecular agglomeration yields a R(residual) that is 0.005, 4−5 times lower than that seen for unimolecular or termolecular agglomeration steps. The reaction product is a black precipitate of Ir(0) metal as the final product "C", eq 3c, consistent with poor stabilization/extensive agglomeration.

The excellent fitting of bimolecular kinetics in a case with extensive agglomeration, one in which we have gone to the opposite extreme of weak anionic stabilization due to the weakly coordinating anion $BF_4^-$, bodes well for the more general applicability of the agglomeration kinetic methods developed herein. Moreover, the system of (1,5-COD)Ir($CH_3CN$)$_2BF_4$ in acetonitrile promises to be of value in rating different stabilizing anions ($Bu_4N^+Y^-$), polymers, and so on in nanoclusters made via eq 1.

The important points here, then, are 3-fold: (i) the generality of eq 1 (i.e., to a wide range of different $Y^-$, $R_4N^+$, solvents, added polymers, and other common nanocluster stabilizers); (ii) the fact that acetonitrile is a coordinating enough solvent that it induces agglomeration and is a important solvent for future agglomeration studies; and especially (iii) kinetic determinations leading to a measure of the rate constant for agglomeration, $k_3$, can now be measured and used to rank *quantitatively* nanocluster stabilizers.

**Scheme 1. Proposed, Minimum Mechanism for the Formation of Ir(0) Nanoclusters Prepared under $H_2$**

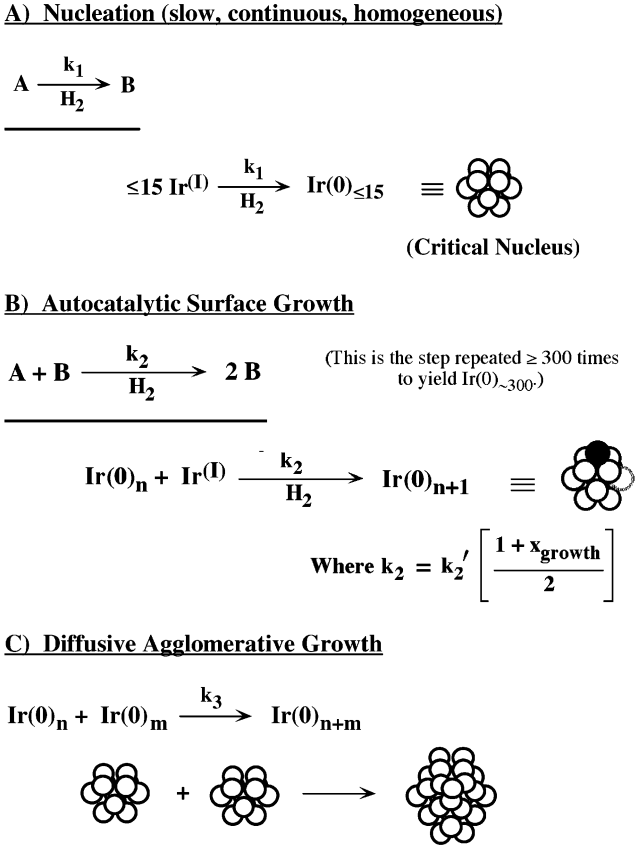


**A Pictorial View of the Proposed, Minimum Mechanism for the Formation of Ir(0) and Other Transition-Metal Nanoclusters Prepared under $H_2$.** The present studies provide the first kinetic evidence in modern transition-metal nanoclusters for the expected step of agglomeration.[1−6,10] While fits to the experimental data, for both the pyridine- and the acetonitrile-induced agglomeration experiments, rule out a first-order agglomeration process (Figure S2 of the Supporting Information), it is important to note that we were able to rule out unequivocally a third-order rate law ($\alpha[B]^n$, $n \geq 3$) only in the case of acetonitrile and the weak stabilizer $BF_4^-$ where agglomeration is more extensive. However, we have applied Occam's Razor since a direct termolecular reaction between nanoclusters is implausible (termolecular reactions are rare, being known primarily only for gas-phase reactions where the third body is required to carry away the heat of the reaction) and since the literature to date writes exclusively a second-order agglomeration process (although, as noted earlier, there is little experimental prior evidence for that second-order rate law).[3−6] In fact, the present work is the first demonstration for modern transition-metal nanoclusters that a second-order process fits the data while a first-order one does not and, for the acetonitrile plus $BF_4^-$ case, that a third-order process is also inferior.

Shown in Scheme 1 is the mechanism we have developed[7a,21d] consisting of three main pseudo-elemen-

tary steps: A → B, slow continuous nucleation, A + B → 2B autocatalytic, surface growth, and 2B → 2(1−*y*)B + 2*y*C (or, when simplified, *y*B → *y*C) agglomeration step.[21] There is some evidence (the percentage cyclooctane evolution at the end of the induction period) for critical nucleus size of ≤Ir(0)$_{\sim 15}$, but much more work is needed to identify the true critical nucleus size as a function of different metals, which appear to have different, inherent critical nucleus sizes.[25]

The mechanism in Scheme 1 is now fully supported by kinetic evidence for each of its three main components, nucleation, growth, and agglomeration. In addition, a kinetic method is now available to study (i) nanocluster formation ($k_1$ and $k_2$) *and* (ii) stability/agglomeration ($k_3$). This promises to be an important advance since it should allow several additional advances: the ready recognition of agglomeration; the measurement of the agglomeration rate constant, $k_3$, and quantitative studies of agglomeration, $k_3$, as a function of all the variables that stabilize or destabilize transition-metal nanoclusters.

Workers using the agglomeration kinetic methods developed herein are reminded of the approximations or assumptions behind the method[22] and its proper use (i.e., the ways to minimize the error in the resultant $k_3$ values cited earlier in the text or in a footnote[22]). The interested reader is referred to an earlier publication for a treatment of the $x_{\text{growth}}$ and "scaling factor" shown in Scheme 1 (an approximation to the changing surface area as the nanocluster grows).[21a] Note also that the $k_2$ and $k_{2'}$ (note the prime) rate constant nomenclature in Scheme 1 updates[26] that provided in the analogous scheme presented elsewhere.[7a,21d]

**Implications for Nanocluster Catalysis: Slowing Bimolecular Agglomeration by Using Low Concentrations of Highly Active Nanoclusters and Insights for the "Is It Homogeneous or Heterogeneous Catalysis?" Question.** An important insight for catalysis by nanoclusters follows from the observation that the nanoclusters deactivate in a bimolecular process whereas catalytic cycles are typically first-order in catalyst concentration. This means that *nanocluster catalytic lifetimes will be improved by using dilute concentrations of highly active nanoclusters*. The observation of (at the time) recored nanocluster catalytic lifetimes[27] for low, ∼$10^{-7}$ concentration of highly active, polyoxoanion-stabilized Rh(0) nanoclusters is consistent with this prediction.

Our demonstration of bimolecular agglomeration also bears on the more general, historically vexing mechanistic issue of "Is it homogeneous vs nanoparticle or other heterogeneous catalysis?"[28] Bimolecular agglomeration means that low concentrations of high activity nanoclusters will have longer catalytic lifetimes. Hence, they can easily go undetected as the true catalysts in ostensibly "homogeneous" reactions.[27,28]

**Unexplained, Interesting Observations on Factors Affecting the Stability of Modern Transition-Metal Nanoclusters.** The observations that (a) pyridine induces agglomeration of even $P_2W_{15}Nb_3O_{62}^{9-}$-stabilized Ir(0) nanoclusters is readily explainable by classical arguments related to DLVO theory type of stabilization:[14] as noted earlier, the pyridine displaces the stabilizing $P_2W_{15}Nb_3O_{62}^{9-}$ (poly)anion from the nanoclusters' surface, resulting in a reduced Coulombic repulsion between particles and, then, enhanced agglomeration. However, unexplained at present are why $P_2W_{15}Nb_3O_{62}^{9-}$-stabilized Ir(0) nanoclusters (b) are not agglomerated by 0.5 M $Bu_4N^+BF_4^-$ or why (c) they and a number of other modern transition-metal nanoclusters[11] apparently do not have a ccc (critical coagulation concentration), that is, why they can be taken to dryness and then completely redissolved without observable agglomeration by TEM. While additional studies with other salts are warranted (e.g., cations such as $Li^+$, $Na^+$, or divalent $Ca^{2+}$ and other anions), there *appear* to be additional, complex,[12] non-DLVO forces[24] at work in stabilizing transition-metal nanoclusters—one of which almost surely is steric stabilization.[14] Understanding better these observations and those forces is an important goal for future work.

## Experimental Section

**Materials.** Unless otherwise reported, all reaction solutions were prepared under oxygen- and moisture-free conditions using a Vacuum Atmospheres drybox (<5 ppm $O_2$ as continuously monitored by a Vacuum Atmospheres $O_2$-level monitor). $[(n\text{-}C_4H_9)_4N]_9P_2W_{15}Nb_3O_{62}$ was prepared according to our most recent procedure from $Na_{12}[P_2W_{15}O_{56}]$ and $NbCl_5$.[29] The $Na_{12}[P_2W_{15}O_{56}]$ was made from our recently optimized synthesis.[30] $[(n\text{-}C_4H_9)_4N]_5Na_3[(1,5\text{-COD})Ir{\cdot}P_2W_{15}Nb_3O_{62}]$, **1**, was prepared as previously described[31] and its purity confirmed by $^{31}$P NMR and elemental analysis (1,5-COD = 1,5-cyclooctadiene). (1,5-COD)Ir$(CH_3CN)_2BF_4$ was prepared according to literature procedure for the corresponding $PF_6^-$ salt.[32] Its purity was confirmed by $^1$H and $^{13}$C NMR. Cyclohexene (Aldrich, 99+%, stabilized with 0.01% 2,6-di-*tert*-butyl-4-methylphenol) was distilled from sodium metal under argon (≤99% purity by GC) and stored in the drybox. Propylene carbonate (Aldrich, 99.7%, anhydrous grade, water <0.005 wt %) was stored in the drybox over activated 5-Å molecular sieves. Pyridine (Aldrich, 99.8%) was distilled from calcium oxide under argon and stored under argon in a 5 °C refrigerator. Acetonitrile (Aldrich 99.93%, HPLC grade) was purged with argon for 30 min and then stored over 5-Å molecular sieves in the drybox. $HBF_4$ (Aldrich, 54 wt % in $Et_2O$) was stored in the refrigerator and handled under an inert atmosphere.

**TEM Experiments.** Transmission electron microscopy (TEM) was performed as before at the University of Oregon with the expert assistance of Dr. JoAn Hudson. Micrographs

(25) Finney, E. E.; Hornstein, B. J.; Finke, R. G. Unpublished results and experiments in progress.

(26) (a) Specifically, the $k_2$(obs) and $k_2$(obs) = $k_2[(1 + x_{\text{growth}})/2]$ used elsewhere[7a,21d] should be updated (replaced) by the $k_2$ and $k_2 = k_2'[(1 + x_{\text{growth}})/2]$ used in Scheme 1 herein. The definitions of $k_1$, $k_2$, and $k_3$ used herein of course as always refer back to specific equations, namely, eqs 3a, 3b, and 3c in the text. (b) This update[26a] still leaves the potential for a bit of confusion for the reader who looks at eq C.5b or C.7b elsewhere[21a] (where the $k_2$ used there, as redefined by eq. C.5b elsewhere,[21d] equals the $k_2'$ used herein); hence, we point out the evolution of our rate constant nomenclature here to minimize that confusion.

(27) Aiken, J. D., III; Finke, R. G. *J. Am. Chem. Soc.* **1999**, *121*, 8803, see the comments on p 8808.

(28) A current review of the "homogeneous or heterogeneous catalysis" issue: Widegren, J. A.; Finke, R. G. *J. Mol. Catal. A* **2003**, *198*, 317−341.

(29) Weiner, H.; Aiken, J. D., III; Finke, R. G. *Inorg. Chem.* **1996**, *35*, 7905−7913.

(30) Hornstein, B. J.; Finke, R. G. *Inorg. Chem.* **2002**, *41*, 2720−2730.

(31) Pohl, M.; Lyon, D. K.; Mizuno, N.; Nomiya, K.; Finke, R. G. *Inorg. Chem.* **1995**, *34*, 1413.

(32) Day, V. W.; Klemperer, W. G.; Main, D. J. *Inorg. Chem.* **1990**, *29*, 2345 and references therein.

of the *soluble portion* of the reaction product solutions were obtained with a Phillips CM-12 microscope (with a 2.0-Å point-to-point resolution) operating at 100 keV. Nanocluster sizes were obtained from micrographs at 430k and 580k magnification.

**Synthesis of Ir(0) Nanoclusters Starting with [($n$-$C_4H_9$)$_4$N]$_5$Na$_3$[(1,5-COD)Ir·P$_2$W$_{15}$Nb$_3$O$_{62}$].** The Ir(0) nanoclusters were synthesized by procedures based on our "Standard Conditions" reaction conditions.[16a,21b,33] Experiments were carried out on an in-house constructed, previously well-described[16a,21b,33] hydrogenation apparatus for continuously monitoring the pressure loss consisting of a Fischer−Porter pressure bottle connected to both a hydrogen line with Swagelock quick-connects and to an Omega pressure transducer that, in turn, is connected to a PC by a White Box A/D converter. Briefly, 20.0 mg of [($n$-$C_4H_9$)$_4$N]$_5$Na$_3$[(1,5-COD)Ir·P$_2$W$_{15}$Nb$_3$O$_{62}$], **1** ($3.53 \times 10^{-6}$ mol) is weighed into a vial in the drybox and dissolved in 2.5 mL of acetone to give a clear yellow solution. Distilled cyclohexene (0.5 mL) was added with a 2.5-mL gastight syringe. The solution was then transferred by a disposable polyethylene pipet to a new 22 × 175 mm borosilicate culture tube containing a new $^5/_{16} \times ^5/_8$ in. Teflon-coated stir bar. (The new culture tube for each experiment is an important part of the apparatus, one that avoids the often more facile heterogeneous nucleation[34] and, therefore, allows reproducible homogeneous nucleation during the nanocluster synthesis.[16a]) The culture tube was inserted into a 100-mL Fischer−Porter bottle, sealed, transferred out of the drybox, and attached to the hydrogenation apparatus referenced above, which is maintained at 22.0 ± 0.1 °C by means of a temperature-controlled water bath. Next, the rapidly stirring solution is purged 15 times with $H_2$ (40 ± 1 psig, 15 s/purge), the pressure is set to 40 ± 1 psig $H_2$, $t = 0$ is noted, and pressure vs time data is collected at 1-min intervals. Complete formation of the Ir(0) nanoclusters was judged by monitoring the evolution of 1 equiv of cyclooctane using our previously published method.

For experiments with pyridine, the Fischer-Porter bottle was purged 13 times with $H_2$ and then an aliquot of pyridine solution (8.6 or 122 mM) was added through the ball-valve of the Fischer-Porter bottle under a flow of $H_2$. The bottle was purged 2 more times with $H_2$, the pressure is set to 40 ± 1 psig, $t = 0$ is noted, and pressure vs time data is collected at 1-min intervals. The evolution of 1 equiv of cyclooctane was also followed by GC as described elsewhere. A plot showing the cyclooctane evolved vs time, Figure S4 of the Supporting Information, shows that ∼16 h are required for the complete reduction of the Ir(I) precursor.

**Estimation of $y$ in Equation 4.** The value of $y$ can be estimated from the catalytic activity of the Ir(0) nanoclusters formed in the presence and the absence of agglomeration (see Appendix A, eq A.9). Under the conditions of this study this translates into the catalytic activity in the presence and absence of pyridine.

A "Standard Conditions" hydrogenation experiment was carried out as described above with 20 mg of **1** dissolved in 2.5 mL of acetone. After the formation of the Ir(0) nanocluster was complete, as judged by the evolution of 1 equiv of cyclooctane by GC, the reaction was stopped and the Fischer-Porter bottle was returned to the drybox. To the same reaction solution was added 1.0 mL of cyclohexene. The culture tube was resealed in the Fischer-Porter bottle and brought from the drybox and a hydrogenation experiment was initiated. Pressure vs time data were collected for 1 h and the initial rate was determined by the well-known methods detailed elsewhere.[18]

Next, the catalytic activity of the nanoclusters formed in the presence of pyridine was determined. Again, a Ir(0) nanocluster synthesis reaction was carried out similar to that above, but the 20 mg of **1** was dissolved in 1.7 mL of acetone and 0.80 mL of a pyridine solution were added (2 equiv based on Ir). This reaction was allowed to go to completion; again the nanocluster formation reaction was monitored by the evolution of 1 equiv of cyclooctane. Once the Ir(0) nanoclusters were completely formed, the Fischer-Porter bottle was returned to the drybox, the pressure was released, and the culture tube was removed from the Fischer-Porter bottle.

To remove the pyridine from the surface of the nanoclusters, 2 equiv (based on Ir) of $HBF_4$ was added to the reaction solution. With the addition of $H^+$, any decrease in catalytic activity should be due to agglomeration and not due to poisoning of the nanocuster surface by pyridine. We have also avoided the possibility of catalyst poisoning by the conjugate base of the added acid by using $BF_4^-$, a classic, weakly coordinating anion.[20] After the acid was added, 1.0 mL of cyclohexene was added to the solution and the mixture was stirred for 5 min in the drybox. The culture tube was returned to the Fischer-Porter bottle, and the bottle was removed from the drybox and attached to the hydrogenation line. As before, the catalytic activity was determined from pressure vs time data over the course of 1 h. Applying the initial rate data treatment as described elsewhere,[18] a value of $B_f = 21.8$ psig $H_2$/h was measured. This value along with the value for $B_o$, determined above, leads to $y = 0.45$ for polyoxoanion-stabilized Ir(0) nanoclusters formed in the presence of 2 equiv of pyridine.

**Synthesis of Ir(0) Nanoclusters Starting with [(1,5-COD)Ir(CH$_3$CN)$_2$]BF$_4$ in Acetonitrile.** In the drybox, 1.7 mg of (1,5-COD)Ir(CH$_3$CN)$_2$BF$_4$ ($3.62 \times 10^{-6}$ mol) was weighed into a 5-mL vial and dissolved in 2.5 mL of $CH_3CN$ to give a clear yellow solution. To this was added 0.5 mL of cyclohexene and 1 equiv of Proton Sponge, which is necessary to neutralize the 1 equiv of $H^+$ evolved in the reduction of the Ir(I) starting material.[15b] The solution was then transferred by a disposable polyethylene pipet to a new 22 × 175 mm borosilicate culture tube containing a new $^5/_{16} \times ^5/_8$ in. Teflon-coated stir bar and placed in the Fischer-Porter bottle. The bottle was sealed, transferred out of the drybox, attached to the hydrogenation line, and purged 15 times with $H_2$ before the pressure was set at 40 ± 1 psig $H_2$ and $t = 0$ was set.

**Fitting of the Resultant Kinetic Data.** Raw pressure vs time data collected with the computer-interfaced transducer, described above, were exported from LabView and imported into MicroCal Origin v. 3.5. Before any fitting was done, the raw data from experiments carried out in acetone or acetonitrile were corrected for the build up of pressure in the Fischer-Porter bottle due to the solvent vapor pressure.[21d] The corrected experimental data were fit with two separate fitting programs, MicroCal Origin v. 3.5 (for $k_{1obs}$ and $k_{2obs}$) and MacKinetics v. 0.9 (for $k_{1obs}$, $k_{2obs}$, and $k_{3obs}$).

Fits with Origin were carried out using the analytic expression for the autocatalytic mechanism derived elsewhere.[21a] Typically, the entire data set was fit to this mechanism; however, for experiments where aggregation was involved, only the first half of the data was used to determine the rate constants for eqs 3a and 3b, $k_{1obs}$ and $k_{2obs}$, respectively.

MacKinetics (equipped with a numerical integration package and a data fitting routine) was then used to fit the complete corrected experimental data set to the full mechanism presented in eqs 3a, 3b, and 3c. Since the fit values obtained from MacKinetics can often be very sensitive to the initial parameters, and since local rather than the desired global minimum is a perennial problem in such multiparameter space searches, initial guesses for $k_{1obs}$ and $k_{2obs}$ were made from a fit of the first half of the data to the autocatalytic mechanism using Origin. This procedure significantly reduced the time required for MacKinetics to obtain a satisfactory fit and, in our experience, leads to more reliable fits—it basically reduces a 3-parameter space search to more of a 1-parameter ($k_{3obs}$) space search. To make the fitting procedure even more efficient, the number of parameters required by MacKinetics was further minimized by replacing eq 3c with B + B → C

(33) Aiken, J. D., III; Finke, R. G. *Chem Mater.* **1999**, *11*, 1035−1047.

(34) For evidence suggesting that heterogeneous nucleation can be a faster, lower energy pathway than homogeneous nucleation in solution, at least in nanocluster formation reactions proceeding by diffusion-controlled steps, see: Strey, R.; Wagner, P. E.; Viisanen, Y. *J. Phys. Chem.* **1994**, *98*, 7748.

(rate constant = $k_{3obs'}$). As shown in Appendix A (eq A.15), this observed rate constant ($k_{3obs'}$) is easily converted to the $k_{3obs}$ rate constant given in eq 3c via the relationship $k_{3obs} = (2/y)k_{3obs'}$. (See the derivation in eq A.10−A.15, Appendix A.)

Some additional notes are in order here about the proper use of MacKinetics and how to avoid local minima. Reading the on-line manual for MacKinetics is an important, required first step (http://members.dcu.net/leipold/mk/mk091.hmtl). [Reading the "bugs" page is also recommended: note the cryptic bug report of the "(Number one bug) Optimization using rate constants as the iteration variable is UNRELIABLE" does *not* mean that MacKinetics cannot be used as it has been herein (a point that our reproducible rate constants make clear and a point that seems obvious by the fact that a curve-fitting routine is a basic component of MacKinetics); it does mean that unmonitored, uncontrolled, and unconstrained (where possible) searches of *n*-dimensional spaces are unreliable!] Noteworthy advice in the on-line manual includes making sure (a) that the fits obtained look visually acceptable when plotted vs the original data, (b) that the residuals from the fits are reasonable, and of course (c) that the fit actually converges: It is important to try many input guesses and to use the gridsearch command to obtain reliable rate constants from the fitting procedure. So far we have found that reliable values have resulted when we (i) used Origin to obtain good initial guesses for (i) $k_{1obs}$ and $k_{2obs}$, (ii) then used the gridsearch command to obtain a good initial idea of $k_{3obs'}$ (with the $k_{1obs}$ and $k_{2obs}$ guesses from Origin as the input values), and (iii) then performed multiple, additional fits with MacKinetics in which higher or lower values of $k_{3obs'}$ (than obtained from (ii)) are used as input, and then higher or lower values of $k_{1obs}$ and $k_{2obs}$ (than obtained from either (i) or (iii)) are used as input, and so on. When the values converged to rate constants that differed by ≤10−20%, and only then, did we conclude that we had obtained a reliable fit. There are also hints in the on-line manual for overcoming searches that become stalled on physically unreasonable negative values for rate constants (exponential mapping of rate constants via "Orphan" variables and/or the use of low starting guesses), although we did not need to use those methods to obtain reproducible rate constants as a part of the present studies. We are in the process of obtaining more experience with $k_3$ fits as we explore this method to evaluate nanocluster stabilizers;[19] hence, we will report further insights or pitfalls we discover in due course.[19] Also available to the interested reader is a listing elsewhere[35] of the original literature to the GEAR and GIT programs that are the precursors to MacKinetics, as well as the proper, Occam's Razor approach to use of numerical integration curve-fitting methods (see footnote 2 elsewhere[35]).

**Acknowledgment.** The TEMs for this work were expertly obtained by Dr. JoAn Hudson at the University of Oregon's Microscopy Center. Lisa Starkey is thanked for collecting and sharing the raw data presented in Figure 6. Financial support was provided by the Department of Energy, Chemical Sciences Division, Office of Basic Energy, Grant DOE FG06-089ER13998.

**Supporting Information Available: Appendix A:** Pseudoelementary step treatment of the kinetics. Figure S1. TEM of the redissolvable portion of polyoxoanion-stabilized Ir(0) nanoclusters made in the presence of 2 equiv of pyridine. Figure S2. (A) Plot of [cyclohexene] vs time for the formation of polyoxoanion-stabilized Ir(0) nanoclusters synthesized from **1**, in the presence of 2 equiv of pyridine. (B) Plot of [cyclohexene] vs time for the formation of polyoxoanion-stabilized Ir(0) nanoclusters synthesized from $[P_2W_{15}Nb_3O_{62}]$·$Ir(CH_3CN)_2BF_4$, in acetonitrile. Figure S3. Plot of [cyclohexene] vs time for the formation of polyoxoanion-stabilized Ir(0) nanoclusters synthesized from **1** in the presence of 7 equiv of pyridine. Figure S4. Plot of cyclooctane evolved vs time that accompanies the conversion of the pre-catalyst, $[(1,5\text{-COD})Ir\cdot P_2W_{15}Nb_3O_{62}]^{8-}$, to Ir(0) nanoclusters in the presence of 2 equiv of pyridine (PDF). This material is available free of charge via the Internet at http://pubs.acs.org.

CM034585I

(35) Lyon, D. K.; Finke, R. G. *Inorg. Chem.* **1990**, *29*, 1787.